Journal of Nuclear Materials 398 (2010) 199–206

Contents lists available at ScienceDirect

Journal of Nuclear Materials

journal homepage: www.elsevier.com/locate/jnucmat

# Effect of tensile stress on cavitation damage formation in mercury

Takashi Naoe [a,*], Hiroyuki Kogawa [a], Yoshihito Yamaguchi [b], Masatoshi Futakawa [a]

[a] J-PARC Center, Japan Atomic Energy Agency, Tokai-mura, Naka-gun, Ibaraki 319-1195, Japan
[b] Nuclear Safety Research Center, Japan Atomic Energy Agency, Tokai-mura, Naka-gun, Ibaraki 319-1195, Japan

A B S T R A C T

Cavitation erosion or so called pitting damage was investigated under tensile stress conditions in mercury. In MW-class liquid metal spallation targets, pitting damage is a critical issue to satisfy required power and/or lifetime of the target vessel. Cavitation occurs by negative pressure which is induced through pressure wave propagation due to proton beam injection. Pitting damage is formed by microjet and/or shock wave during cavitation bubble collapse. A mercury target vessel suffers tensile stress due to thermal stress or welding. In order to investigate the effect of tensile stress on pitting damage formation, cavitation erosion tests were performed using stress imposed specimens in mercury. An ultrasonic vibratory horn and electro-Magnetic IMpact Testing Machine (MIMTM) were used to vary the cavitation intensity. In the incubation period of pitting damage, damaged area was slightly increased with increasing imposed tensile stress. In the steady state period, a mean depth of erosion was increased by the tensile stress. Additionally, in order to quantitatively evaluate the effect of tensile stress, an indentation test with Vickers indenter was carried out to quasi-statically simulate the impact load. From the measurement of the diagonal length of the indent aspect ratio and hardness, it is recognized that the threshold of the deformation, i.e. pitting damage formation, was decreased by the tensile stress.



## 1. Introduction

Cavitation phenomena are very dependent on the liquid properties [1–3]. Liquid mercury was selected as a spallation target material for the Japan Spallation Neutron Source (JSNS) taking account of the advantages of neutron yield and self-circulation heat removal efficiency [4,5]. In JSNS highly intense proton beams (3 GeV, 1 MW, 1 μs pulse duration) hit the target at a repetition rate of 25 Hz. Cavitation is induced by the negative pressure through the pressure wave propagation which is caused by thermal shock in mercury, and the pitting damage is formed on the target vessel wall due to cavitation bubble collapse [6,7]. At the same time, the target vessel suffers tensile stresses due to the thermal stress by the proton beam injection [8]. Since the target vessel is fabricated by welding, weld residual stresses are imposed nearby welding lines. In general, tensile stress can cause undesirable effects on a structural integrity, e.g. the fatigue strength degradation and the enhancement of liquid metal embrittlement [9].

The JSNS target vessel is a thin-wall structure to reduce thermal stress; i.e. the thickness of the proton beam window is set to be 2.5 mm. In the previous studies, the authors investigated pitting damage formation and suggested the fatigue strength is remarkably degraded with the growth of pitting damage [10,11]. In this study, the effects of tensile stresses on the pitting damage formation were investigated through the cavitation erosion tests in mercury. Additionally, a quasi-static investigation was performed by the microindentation technique to quantitatively evaluate the effect of tensile stress on the damage formation.

## 2. Experimental

### 2.1. Vibratory horn

From the viewpoint of cavitation intensity, two types of testing machines were used. One is a vibratory horn and the other is the electro-Magnetic IMpact Testing Machine (MIMTM). Cavitation intensity might be dependent on the period of imposed negative pressure, which is ca. 25 μs for the vibratory horn and ca. 1.5 ms for the MIMTM.

Fig. 1 shows the experimental apparatus of the vibratory horn. The apparatus consists of the ultrasonic vibratory horn (NIHONSEIKI, US-1200TCVP), a mercury chamber, a device to impose the tensile stress to the specimen, and a control unit for the vibrational amplitude and the temperature of mercury. The maximum power and vibratory frequency of the horn are 1200 W and 19.5 kHz, respectively. The horn is made of titanium to prevent its own erosion. The amplitude of horn is controlled to be 30 μm through the test. The chamber is filled with ca. 500 $cm^3$ mercury and the cover gas, air, at atmospheric pressure. A water jacket with water

* Corresponding author. Tel.: +81 29 284 3716; fax: +81 29 282 6712.
E-mail address: naoe.takashi@jaea.go.jp (T. Naoe).

0022-3115/$ - see front matter © 2009 Elsevier B.V. All rights reserved.
doi:10.1016/j.jnucmat.2009.10.033

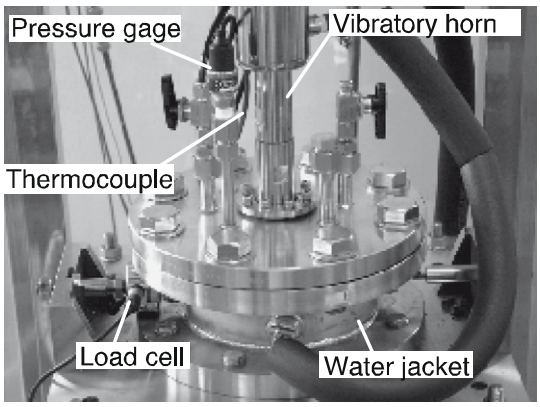


(a) Photograph of ultrasonic vibratory horn

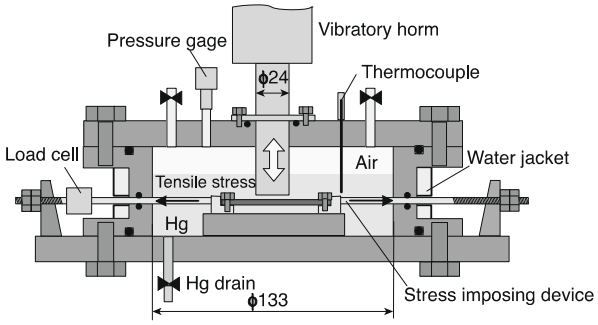


(b) Schematic illustration of mercury chamber

**Fig. 1.** Experimental apparatus of the vibratory horn.

circulation was installed in the mercury chamber to keep the mercury temperature constant around 20 °C.

The specimen was made of type 316L stainless steels which is the structural material of the JSNS mercury target vessel. Fig. 2 shows a schematic drawing of the specimen and the stress imposing device. The size of the specimen is 30 mm in width, 60 mm in length, and 2.5 mm in thickness. The specimen surface was polished using 1 μm buff. The erosion test was performed by the stationary specimen method, i.e. the specimen was held stationary below the vibrating horn as shown in Fig. 1b. This has advantage for specimen to be acceleration-insensitive and as simple as the button type test as conforming to ASTM Standard G-32-98 [12]. The distance between the horn tip and the specimen surface affects pitting damage formation. Distance between the horn tip and the specimen surface in this experiment was set constant at 2 ± 0.1 mm.

In order to investigate the correlation between pitting damage formation and tensile stress, the stress imposing device was installed in the mercury chamber as shown in Fig. 1b. Tensile stress was imposed by rotating the screws connected to the specimen, that is, a displacement controlled system. Imposed stresses were changed within the elastic region equivalent to 0, 100, and 200 MPa, and testing time was 10 and 20 min, respectively. Mercury temperature and imposed load were measured by a thermocouple and a load cell. Each specimen was washed in an ultrasonic bath with an ethanol after test to observe the damaged surface.

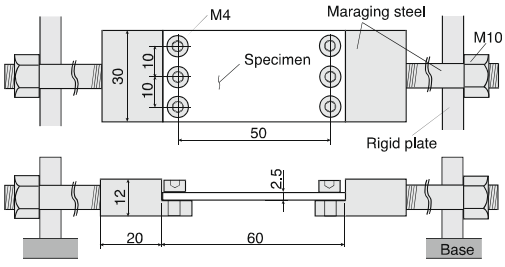


**Fig. 2.** Schematic drawing of the specimen and the device to impose the tensile stress.

### 2.2. MIMTM

The electro-Magnetic IMpact Testing Machine (MIMTM) tests were performed to investigate the effect of tensile stress on the pitting damage. Fig. 3 shows the experimental apparatus of the MIMTM test. Cavitation was produced in the mercury chamber of 100 mm in inner diameter by mechanically induced pressures through the electromagnetically driven striker. Imposed power to electromagnetic coil and repeated frequency were 560 W/pulse and 25 Hz, respectively. The amplitude of striker in this experiment is ca. 300 μm. More detailed information of the MIMTM was described in Ref. [10]. Specimen material was type 316 stainless steel and tensile stress was imposed by the four points bending jig which was installed in the upper flange of the mercury chamber. The size of the specimen is 4 mm in width, 60 mm in length, and 2.5 mm in thickness. Imposed stress was changed 0 MPa and 190 MPa, as determined by:

$$W = \frac{6EI(T-t)}{\left(\frac{L-l}{2}\right)^3\left(\frac{6l}{L-l}+2\right)} \quad (1)$$

$$\sigma_{b4} = \frac{3W(L-l)}{bh^2} \quad (2)$$

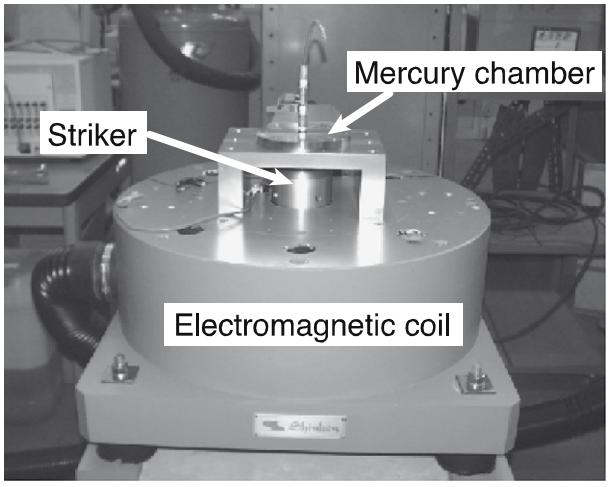


(a) Photograph of MIMTM

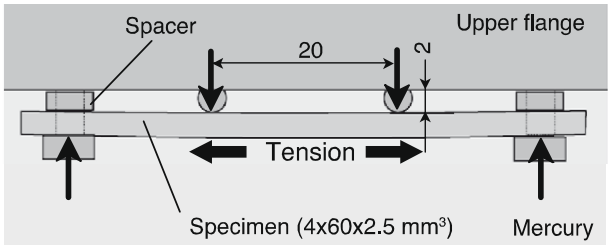


(b) Schematic drawing of specimen and jig

**Fig. 3.** Experimental apparatus of the electro-Magnetic IMpact Testing Machine.

where, $W$ is the load at each of support point, $E$ the Young's modulus, $I$ the second moment of area, $T$ the inner span height, $t$ the spacer thickness, $L$ and $l$ the outer and inner spans, $\sigma_{b4}$ the stress, $b$ the specimen width, and $h$ the specimen thickness. The number of impacts were $10^5$, $10^6$, $5 \times 10^6$, and $10^7$.

## 3. Results

### 3.1. Vibratory horn

#### 3.1.1. Mercury temperature

Fig. 4 shows the change in mercury temperature during 20 min tests under 100 and 200 MPa conditions. Before the test mercury temperature was kept to be at 11 °C by water. Immediately after the vibration started, the temperature gradually increased with testing time, and after 5 min the temperature became constant at 18 °C.

Liquid temperature can affect pitting damage formation [13,14]. In order to investigate the effect of the temperature change on cavitation damage, liquid properties dependent on temperature were examined. From the viewpoint of bubble dynamics, liquid properties that can affect cavitation bubble behavior are density, surface tension, viscosity, and vapor pressure. In this experimental temperature range, however, even the vapor pressure – the property which is most sensitive to the temperature – is hardly affected on bubble behavior [15]. Therefore, the effect of mercury temperature change in this experiment was ignored.

#### 3.1.2. Damage measurement

Fig. 5 shows the damaged specimen surface after 10 min test at 100 MPa condition. In the figure, arrows denote the loading direction. Pitting damage is concentrated just under the horn tip. Furthermore, the damage at the horn edge was more violent than that at center. In this experiment the damage observation was focused on approximately 16 mm$^2$ around the specimen center taking account of the damage distribution as shown in Fig. 5.

Fig. 6 shows microscopic images of the specimen surface taken by a laser microscope (LASERTECH, LHD-15H) after 10 and 20 min tests at various loading conditions. The arrows in the figure denote loading direction. It is recognized that the number of the visible pits are increased with not only testing time but also the increasing in imposed tensile stress.

In order to quantitatively investigate pitting damage formation the fraction of eroded area is defined as $A_e/A_0$, where $A_0$ is the measured area and $A_e$ is the eroded area that is estimated by the laser microscope images [10]. In this experiment, the eroded areas were estimated taken over five sampled fields (the area of a field = 1.05 × 0.79 mm$^2$) around the specimen center. Fig. 7 shows the relationship between the measured eroded area and the imposed tensile stress. The eroded areas were increased with the increasing in imposed tensile stress. In the 10 min test at 200 MPa condition, the eroded area was increased approximately double in the 0 MPa condition.

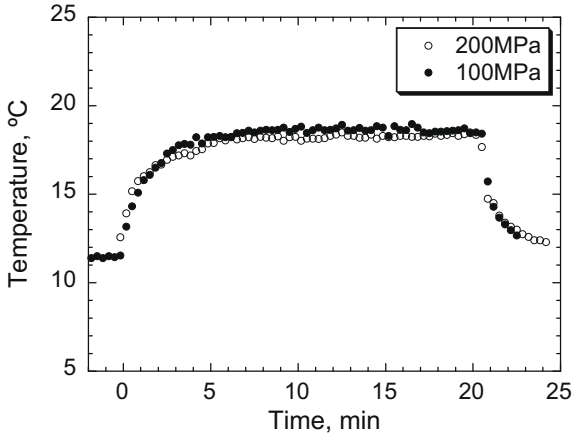


**Fig. 4.** Change in mercury temperature at 20 min vibratory horn tests.

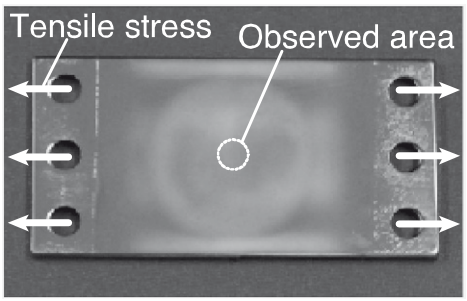


**Fig. 5.** Macroscopic image of specimen surface after 10 min test at 100 MPa.

#### 3.1.3. Depth of the pits

As mentioned above, pitting damage was increased by the imposed tensile stress. Here, we focused on the depth profile of the pits in order to investigate why the damaged area was increased due to the imposed tensile stress. Fig. 8 shows the typical depth contour of the specimen surface and the depth profiles of the pits taken by a laser microscope (KEYENCE, VK-9510). The depth profiles were measured from the contours as indicates dash line on the depth contour in parallel with loading direction. It is recognized that the pit depth was hardly changed by the imposed stress. Fig. 9 shows the relative frequency distribution of the maximum pit depth measured from more than 50 pits. The peak value and distribution were hardly changed due to the imposed stress. Fig. 10 shows equivalent pit diameter distribution and its cumulative relative frequency. The equivalent pit diameter was measured from the binarized image which was used for the eroded area estimation, and the pits of less than 3 μm in diameter were ignored as taking account of the noise. It is recognized that the number of the pits in each diameter range is increased with increasing in imposed stress, especially as mentioned cumulative relative frequency, the percentage of the large pits is increased. Therefore the increase of the fraction of eroded area by the tensile stresses is caused by the increasing of the number and size of the pits.

### 3.2. MIMTM tests

#### 3.2.1. Damage observation

Fig. 11 shows macroscopic images of the damaged specimens after several impacts at 190 MPa condition. The damage observation was focused on the center of the specimen.

Fig. 12 shows microscopic images of the specimen surface taken by the laser microscope and its depth profiles after $10^5$ and $5 \times 10^6$ impacts. The depth profiles were measured on the dash line shown in images. After $10^5$ impacts, the difference between the 0 MPa and the 190 MPa conditions were hardly recognized as mentioned the vibratory horn tests. On the other hand, after $5 \times 10^6$ impacts the maximum depth of the 190 MPa condition was deeper than that of the 0 MPa condition although an original surfaces of the both specimens were not recognized due to the overlapped pits. From the depth profile, the peak to peak roughness was measured. Fig. 13 shows relationship between the peak to peak roughness and the number of impacts. The roughness was an average value of the five typical large pits which measured in 3 mm$^2$ area around the specimen center. In less than $10^6$ impacts, it is recognized that

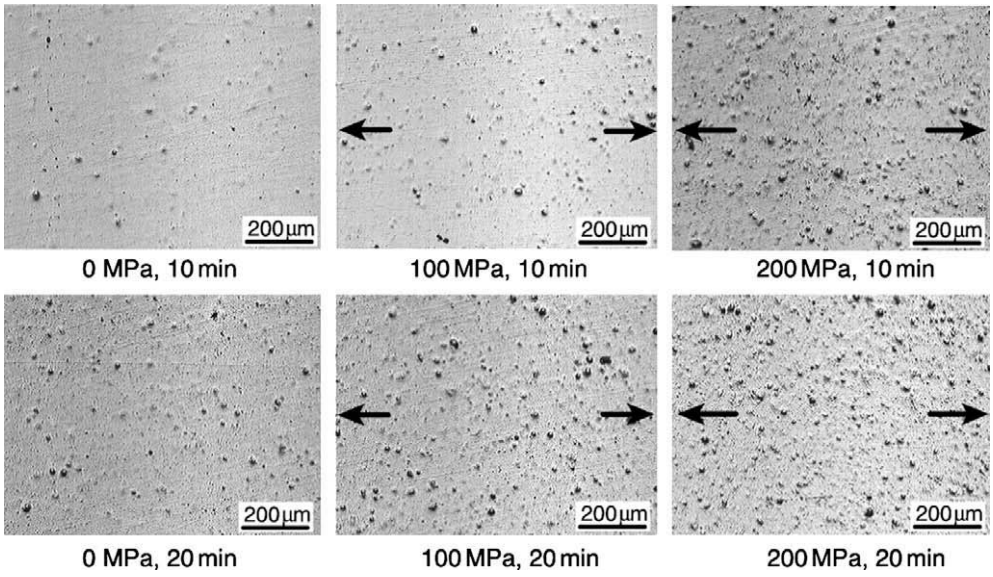


**Fig. 6.** Micrographs of specimen surface taken by a laser microscope after 10 and 20 min tests at various loading conditions. The arrows denote loading directions.

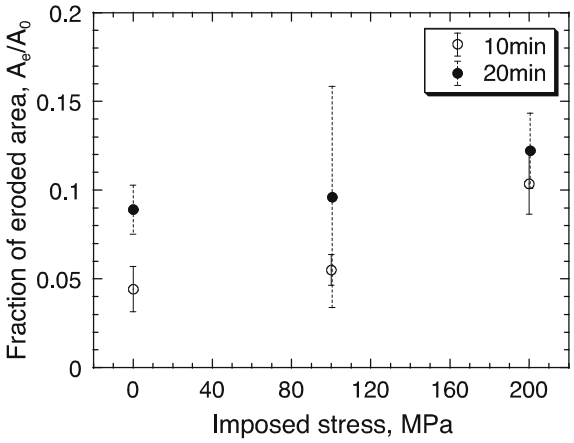


**Fig. 7.** Change in the fraction of eroded are as a function of imposed tensile stress.

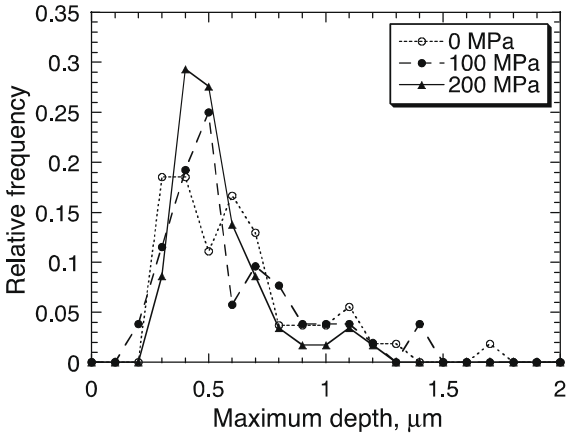


**Fig. 9.** Relative frequency distribution of the maximum pit depth.

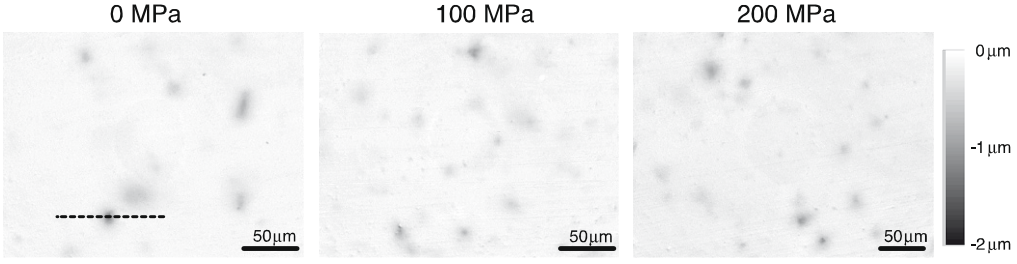


(a) Depth contour of the specimen surface

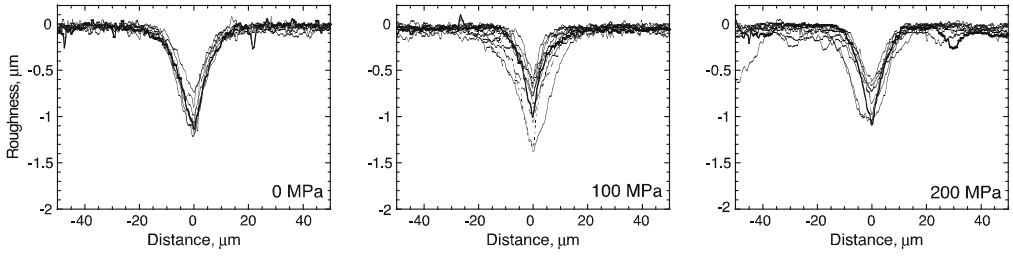


(b) Depth profiles of the pits

**Fig. 8.** Typical depth contour of the specimen surface taken by a laser microscope and its depth profiles of the pits.

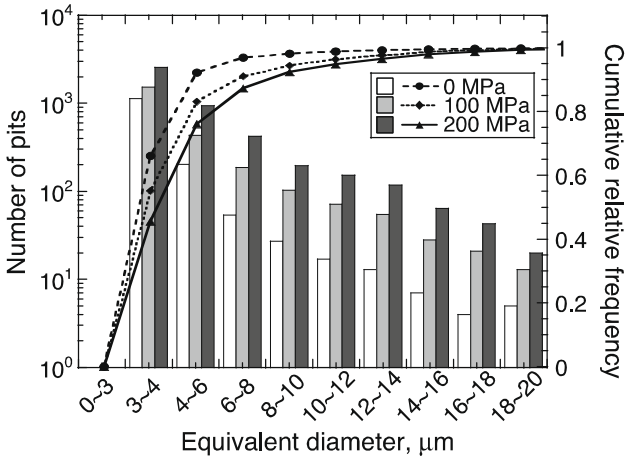


**Fig. 10.** Distribution of equivalent pit diameter in various tensile stresses. It is note that pits of less than 3 μm in diameter were ignored taking account of noise.

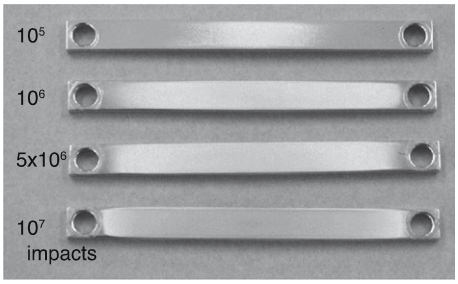


**Fig. 11.** An example image of the damaged specimen at 190 MPa condition.

the peak to peak roughness is slightly increased by the tensile stress. However, over $5 \times 10^6$ impacts the roughness varied widely.

In order to quantitatively compare the pitting damage in a large number of impacts the mean depth of erosion *MDE* was defined as $MDE = w/\rho A$, where $w$ is the weight loss, $\rho$ the density, and $A$ the surface area of the specimen. Fig. 14 shows the relationship between the mean depth of erosion and the number of impacts. In the case of less than $10^6$ impacts, the difference of *MDE* caused by the tensile stress was hardly recognized because the plastic deformation was dominant without any weight loss. On the other hand, more than $5 \times 10^6$ impacts, *MDE* of the 190 MPa condition was clearly increased by comparison with 0 MPa condition.

Fig. 15 shows cross-sections of the specimens after $10^6$ and $10^7$ impacts. Electrochemical etching was performed with saturated oxalic acid to clearly the cracks. In 190 MPa condition, especially, after $10^7$ impacts many cracks were observed at bottom of the pits. Therefore, tensile stress might enhance the crack propagation and accelerate the *MDE*.

## 4. Discussion

### 4.1. Indent

In the vibratory horn tests, the eroded was area increased by tension. In order to evaluate the effect of tensile stress on deformation, i.e. pitting damage formation, quasi-statically estimation was performed using the microindenter.

Microindentation test was performed by the Vickers hardness tester (MATSUZAWA, MHT-2) under the tensile stress conditions. The four points bending jig for the MIMTM tests was used in the indentation tests to impose the tensile stress on the specimen. Indent load was set to 4.9 N by which indent depth corresponding to the pit depth after $10^5$ impacts was formed. Fig. 16 shows typical image of the indent under 170 MPa condition. Diagonal lengths of the indents were measured separately in axial and orthogonal directions against the loading direction as shown in Fig. 16, and the Vickers hardness was estimated.

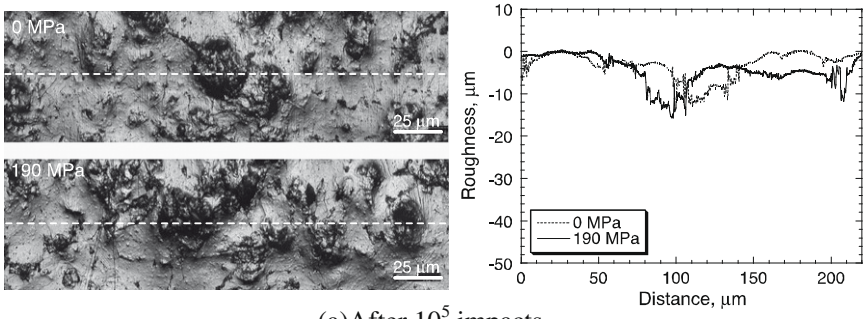


(a)After $10^5$ impacts

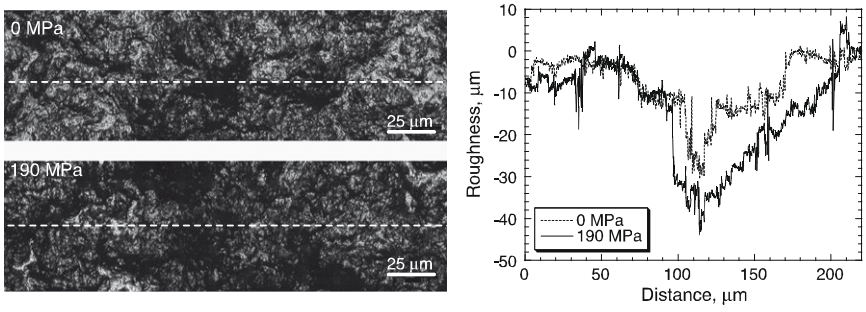


(b)After 5 x $10^6$ impacts

**Fig. 12.** Microscopic images of the damaged surface and its depth profiles taken by the laser microscope after $10^5$ and $5 \times 10^6$ impacts.

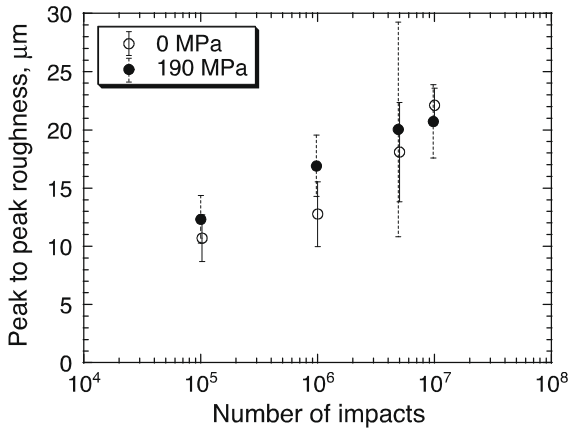


**Fig. 13.** Relationship between the peak to peak roughness and the number of impacts.

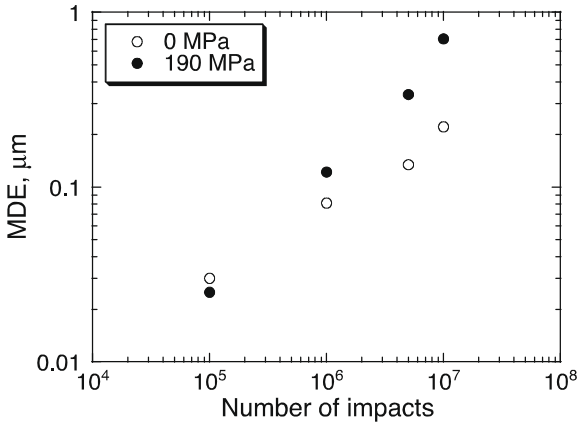


**Fig. 14.** Relationship between the mean depth of erosion and the number of impacts.

Fig. 17 shows the relationship between the aspect ratio (axial/orthogonal) of the indent under loading conditions, the Vickers hardness, and the imposed tensile stress. Each point in the figure is an average of five indents. The aspect ratio of the indent was slightly increased with the imposed stress. Furthermore, the hardness decreased with increasing imposed stress, that is, the indent expanded along the loading direction. This is interpreted that the threshold of the impact for forming pitting damage decreases by increasing tensile stress. Therefore, the pitting damage in the incubation period is enhanced by the tensile stress.

The change in the aspect ratios of the pits from imposed stress was also compared. Fig. 18 shows the relationship between the aspect ratio and the depth of the pits after 10 min vibratory horn tests. The aspect ratios of the pits were slightly increased with the imposed tensile stress. This trend is the same shown in Fig. 17.

### 4.2. Incubation period

The effect of tensile stress on the lifetime of the target vessel was estimated. The morphology of the pitting damage is classified as the *incubation period* or the *steady state*, the former case is

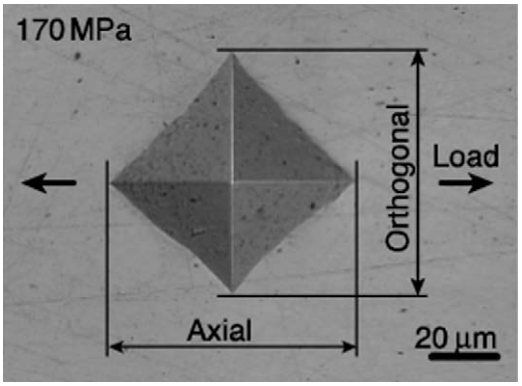


**Fig. 16.** Micrograph of Vickers indent under loading conditions.

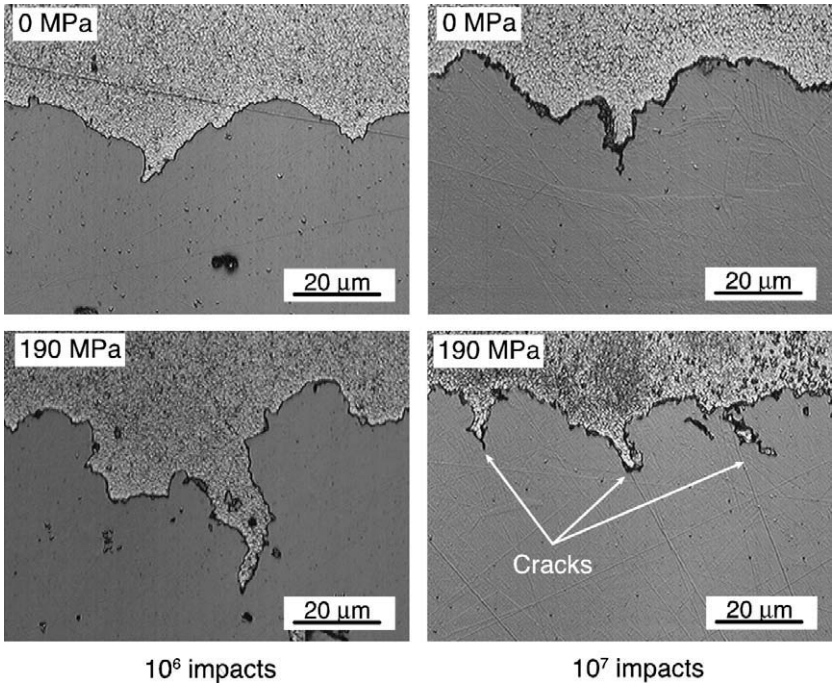


**Fig. 15.** Cross-sections of the specimens after $10^6$ and $10^7$ impacts.

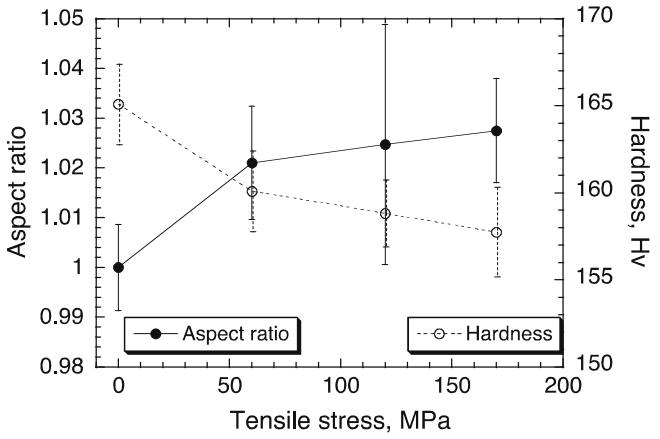


**Fig. 17.** Relationship between aspect ratio (axial/orthogonal) of the indent diagonal length, the Vickers hardness, and the imposed tensile stress.

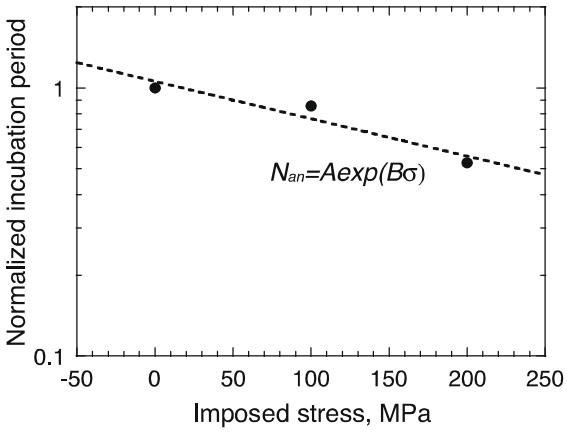


**Fig. 19.** Relationship between normalized incubation period and imposed tensile stress.

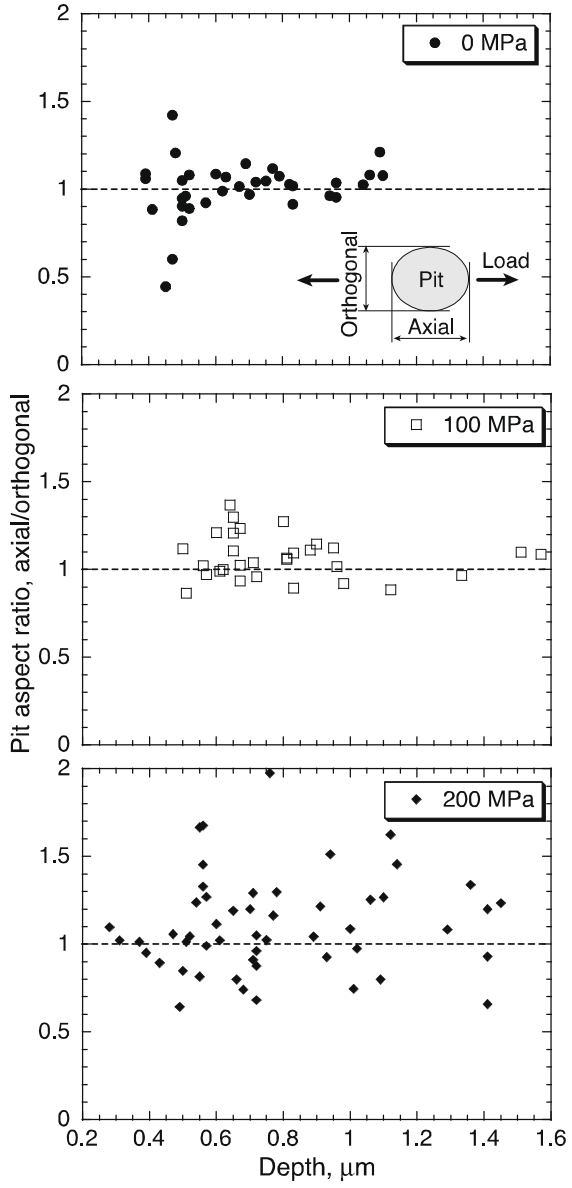


**Fig. 18.** Relationship between aspect ratio (axial/orthogonal) and depth of the pits after 10 min vibratory horn tests.

plastic deformation and the latter case is homogeneous erosion with the weight loss. In the previous study, under non-stress condition it was estimated that the increasing rate of the *MDE* is approximately constant independent of materials and testing conditions [10]. The weight loss starts after the fraction of eroded area reaches nearly 1. Therefore, the estimation of the incubation period is useful in the lifetime assessment of the target vessel.

The incubation period is calculated from the following equations,

$$F_N = 1 - \exp(CN) \tag{3}$$

$$N_a = \frac{\ln(1-0.98)}{C} \tag{4}$$

where, $N$ is the number of impacts, $F_N$ the fraction of eroded area after $N$ impacts, $C$ the constant, and $N_a$ the number of impacts to complete the incubation period [10,16]. Fig. 19 shows the relationship between the estimated incubation period of the vibratory horn test and the imposed tensile stress. The incubation period was normalized at the 0 MPa condition. The decreasing of the normalized incubation period, $N_{an}$, due to the tensile stress was estimated as follows

$$N_{an} = A\exp(B\sigma) \tag{5}$$

where $A$ and $B$ are constants depends on the material and the testing conditions. In the case of our vibratory horn tests, $A$ and $B$ were estimated to be 1.06 and $3.21 \times 10^{-3}$, respectively. The incubation period was slightly decreased with the increasing in the imposed tensile stress, therefore the lifetime of the target vessel will be decreased by the tensile stress. In the case of 200 MPa, the incubation period decreases approximately half of the 0 MPa condition.

## 5. Conclusion

The effect of the tensile stress on the pitting damage formation in the mercury was investigated through the vibratory horn and MIMTM tests.

(1) During the incubation period of the pitting damage, pitting damage as evaluated by the fraction of eroded area increased slightly with the increasing imposed tensile stress because the impact threshold for pitting damage was decreased due to the imposed tensile stress.
(2) In the steady state, it is clearly recognized that the mean depth of erosion as calculated by weight loss was increased by the imposed tensile stress. The tensile stress enhances crack propagation and accelerates erosion.

(3) The change in the incubation period due to tensile stress was estimated. The estimated incubation period in the stress condition near yield is approximately half of the non-stress condition.

## Acknowledgements

The authors thank to Mr. R. Osone of graduate school of Ibaraki University for help damage tests. This work was partly supported by the Japan Society for the Promotion of Science through the Grant-in-Aid for Scientific Research (No. 20360090).

## References

[1] S. Hattori, F. Inoue, K. Watashi, T. Hashimoto, Wear 265 (2008) 1649.
[2] R. Garcia, F.G. Hammitt, Trans. ASME J. Basci Eng. (1967) 753.
[3] M.D. Kass, J.H. Whealton, N.E. Clapp Jr., J.R. Distefano, J.H. DeVan, J.R. Haines, M.A. Akerman, T.A. Gabriel, Tribol. Lett. 5 (1998) 231.
[4] L.K. Mansur, J.R. Haines, J. Nucl. Mater. 356 (2006) 1.
[5] Y. Ikeda, J. Nucl. Mater. 343 (2005) 7.
[6] M. Futakawa, H. Kogawa, R. Hino, H. Date, H. Takeishi, J. Impact Eng. 28 (2003) 123.
[7] B.W. Riemer, J.R. Haines, J.D. Hunn, D.C. Lousteau, T.J. McManamy, C.C. Tsai, J. Nucl. Mater. 318 (2008) 93.
[8] T. Wakui, M. Futakawa, H. Kogawa, Y. Ikeda, J. Nucl. Sci. Technol. 44 (2007) 530.
[9] For example R.W. Staehle, Mater. Sci. Eng. 25 (1976) 207.
[10] M. Futakawa, T. Naoe, C.C. Tsai, H. Kogawa, S. Ishikura, Y. Ikeda, H. Soyama, H. Date, J. Nucl. Mater. 343 (2005) 70.
[11] M. Futakawa, T. Naoe, H. Kogawa, M. Teshigawara, Y. Ikeda, J. Nucl. Mater. 356 (2006) 168.
[12] ASTM Designation G-32-98, American Society for Testing and Materials, 2001, p. 1.
[13] S. Hattori, Y. Goto, T. Fukuyama, Y. Yagi, M. Murase, Wear 260 (2006) 1217.
[14] S.J. Pawel, E.T. Manneschmidt, J. Nucl. Mater. 318 (2003) 122.
[15] T. Naoe, M. Futakawa, T. Koyama, H. Kogawa, J. JSEM 6 (2006) 301 [in Japanese].
[16] H. Soyama, M. futakawa, Tribol. Lett. 17 (2004) 27.